Supporting information

Improved electrochemical performance for high voltage spinel $LiNi_{0.5}Mn_{1.5}O_4$ modified by supercritical fluid chemical deposition

Gwenaëlle COURBARON[a,b], Emmanuel PETIT[a,c], Jon SERRANO-SEVILLANO[a a,d,e], Christine LABRUGÈRE-SARROSTE [f], Jacob OLCHOWKA[a,c,d], Dany CARLIER[a,c,d], Nathalie DELPUECH[b,c,d], Cyril AYMONIER[a,c] * and Laurence CROGUENNEC[a,c,d] *

[a] *Univ. Bordeaux, CNRS, Bordeaux INP, ICMCB, UMR 5026, F-33600 Pessac, France*

[b] *Renault SAS, Technocentre, 1 avenue du golf, 78280 Guyancourt, France*

[c] *RS2E, Réseau Français sur le Stockage Electrochimique de l'Energie, FR CNRS 3459, France*

[d] *ALISTORE-ERI European Research Institute, FR CNRS 3104, 80039 Amiens Cedex France*

[e] *Centro de Investigación Cooperativa de Energías Alternativas (CIC energiGUNE), Basque Research and Technology Alliance (BRTA), Parque Tecnológico de Álava, Albert Einstein 48, 01510 Vitoria-Gasteiz, España*

[f] *PLACAMAT, UAR 3626, CNRS Université Bordeaux, 33600 Pessac, France*

* corresponding authors: Laurence Croguennec (laurence.croguennec@icmcb.cnrs.fr) and Cyril Aymonier (cyril.aymonier@icmcb.cnrs.fr)

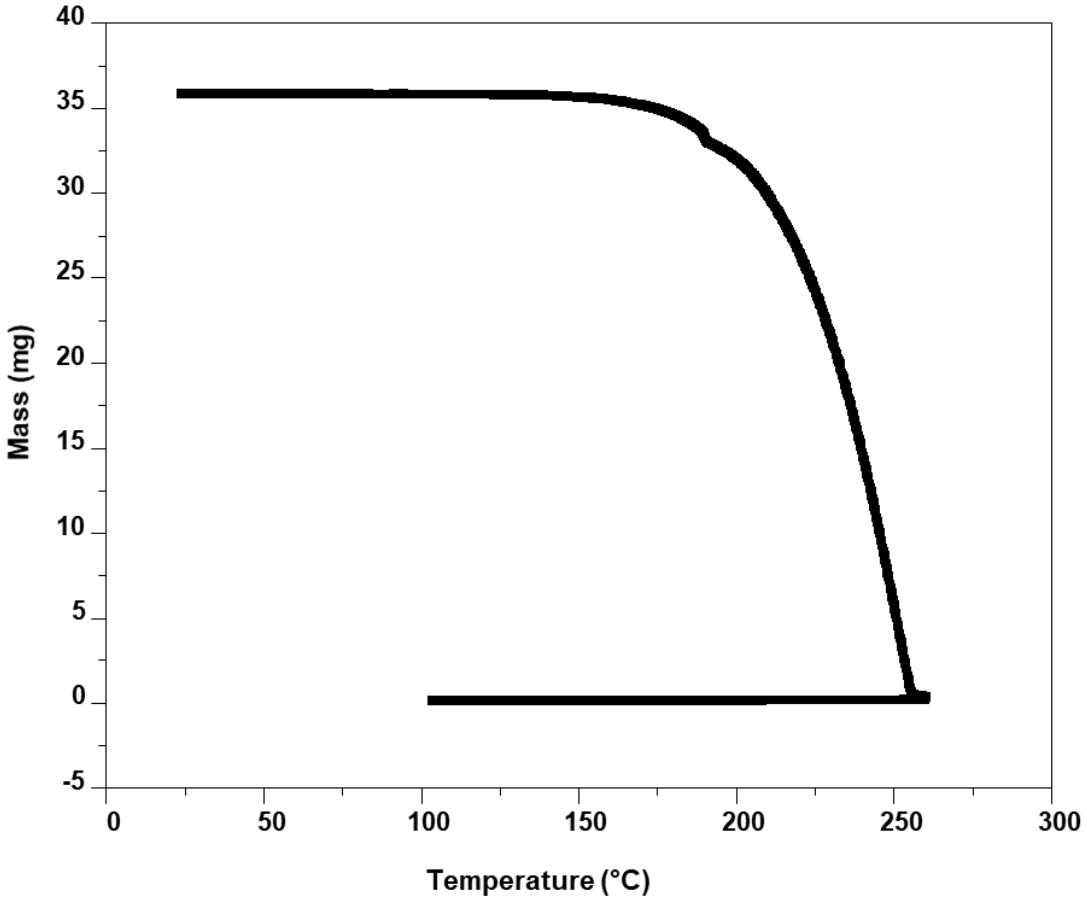

Figure S1 : Thermogravimetric analysis of the precursor $Al(acac)_3$ until 260°C at 5°C/min under air

Table S1: Chemical analyses of transition metals in the spinel: Mn and Ni for bare LNMO and LNMO coated by SFCD and dispersion processes. ICP-OES analyses of coated and reference materials were performed to determine if there is a change in the Mn/Ni ratio after the formation of the coating. The expected Mn/Ni ratio is 3. The atomic content obtained for Mn and Ni and the ratio between both are given below. The 5 mol.% obtained either by SFCD or dispersion route exhibits a Mn/Ni ratio of 3.12 ± 0.05 and 3.25 ± 0.13, respectively versus 2.92 for the pristine material. Surprisingly, a slight increase of the Mn/Ni ratio is observed for the coated materials. We tested several digestion routes and concluded to a matrix effect due to the additional presence of the Al-rich coating for the modified LNMO materials. Indeed, the XRD patterns and electrochemical curves, that are highly sensitive to the spinel composition, are not modified at all.

Sample	Mn atomic content (mol)	Ni atomic content (mol)	Mn/Ni atomic ratio
SFCD 5%_1	1.519 ± 0.003	0.481 ± 0.003	3.15 ± 0.03
SFCD5%_2	1.508 ± 0.002	0.492 ± 0.002	3.07 ± 0.01
DIS 5%_1	1.537 ± 0.005	0.463 ± 0.005	3.32 ± 0.05
DIS 5%_2	1.522 ± 0.002	0.478 ± 0.002	3.19 ± 0.02
Bare LNMO	1.485 ± 0.004	0.515 ± 0.004	2.88 ± 0.04

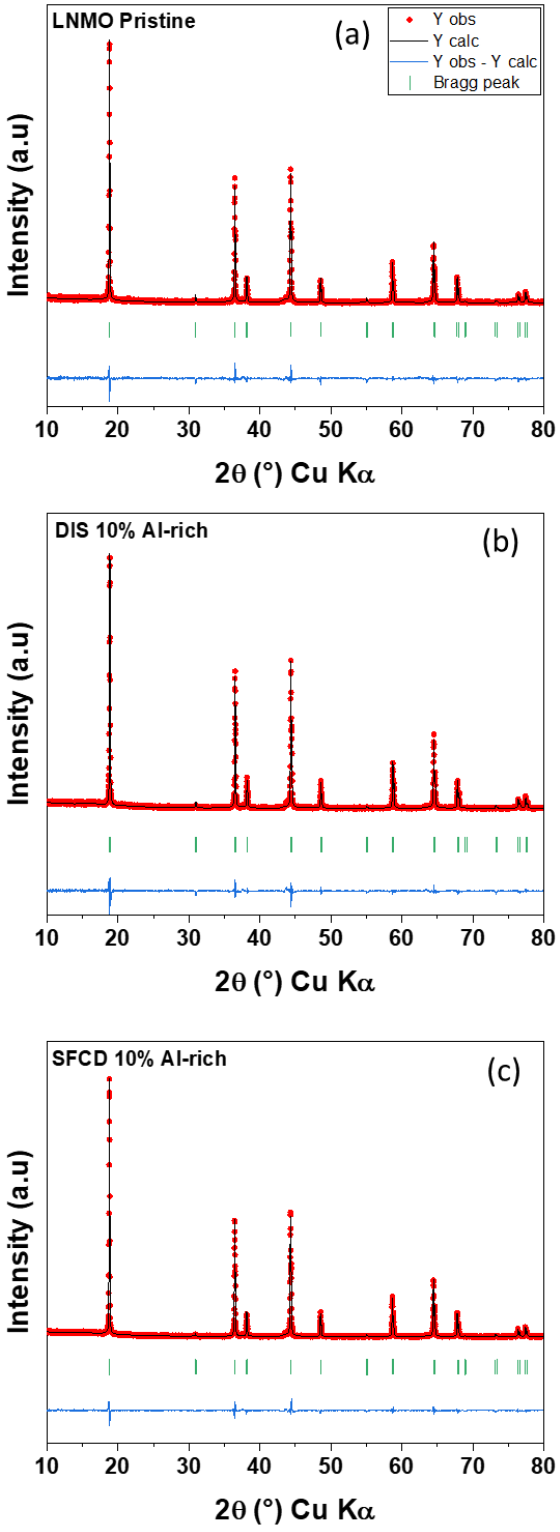

Figure S2: Le Bail refinements given as examples for the pristine LNMO (a), the samples coated with 10 mol.% of Al_2O_3-type obtained either by a dispersion process followed by a thermal treatment (b) or by a supercritical fluid-based process (c).

Table S2: Refined lattice parameters and cell volumes determined by Le Bail refinement using a *Fd-3m* space group for pristine LNMO and coated materials obtained either by a dispersion process followed by a thermal treatment (DIS) or by a supercritical fluid-based process (SFCD).

Sample	**Cell parameter (Å)**	**Volume (Å^3)**
Pristine LNMO	8.1714(4)	545.61(5)
SFCD 0.1%	8.1719(3)	545.72(4)
SFCD 10%	8.1719(3)	545.72(4)
DIS 0.5%	8.1722(4)	545.79(5)
DIS 10%	8.1724(4)	545.81(5)

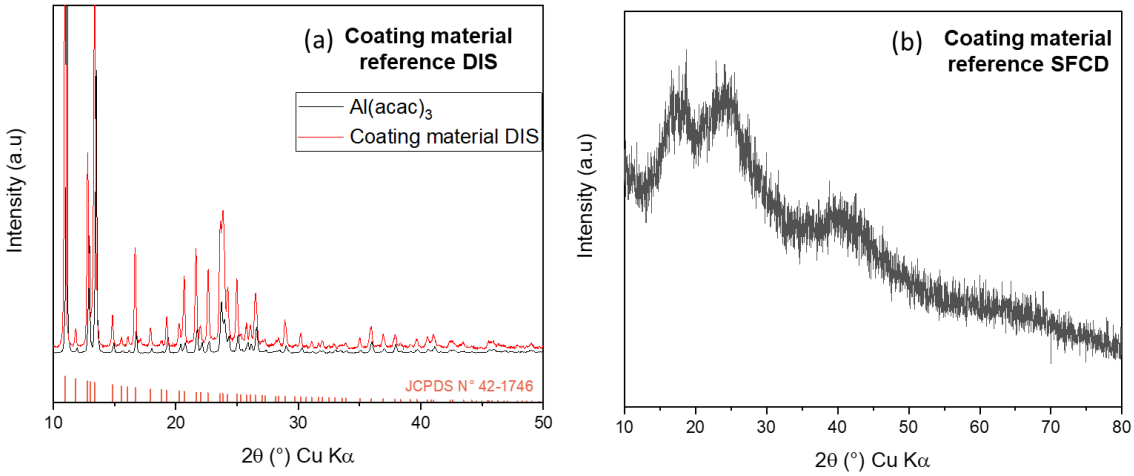

Figure S3: XRD patterns collected for the samples obtained from the decomposition of $Al(acac)_3$ alone in the conditions used for the formation of the coatings by both processes. In the case of dispersion (a), the $Al(acac)_3$ precursor was dissolved in absolute ethanol, the pH value was adjusted to 12 using NH_3 and the solution was stirred for one night (12h) before solvent evaporation and powder heat treatment at 260°C for 2h. The obtained XRD pattern mainly contains the peaks characteristic of the $Al(acac)_3$ precursor (JCPDS N° 42- 1746). In SFCD conditions (b), the $Al(acac)_3$ precursor was dissolved in absolute ethanol, and the solution was stirred for one night and poured into the reactor at 170°C, 200 bars adding CO_2 for 1h. The resulted powder was analysed by XRD and an amorphous material was obtained which could correspond to amorphous alumina[1].

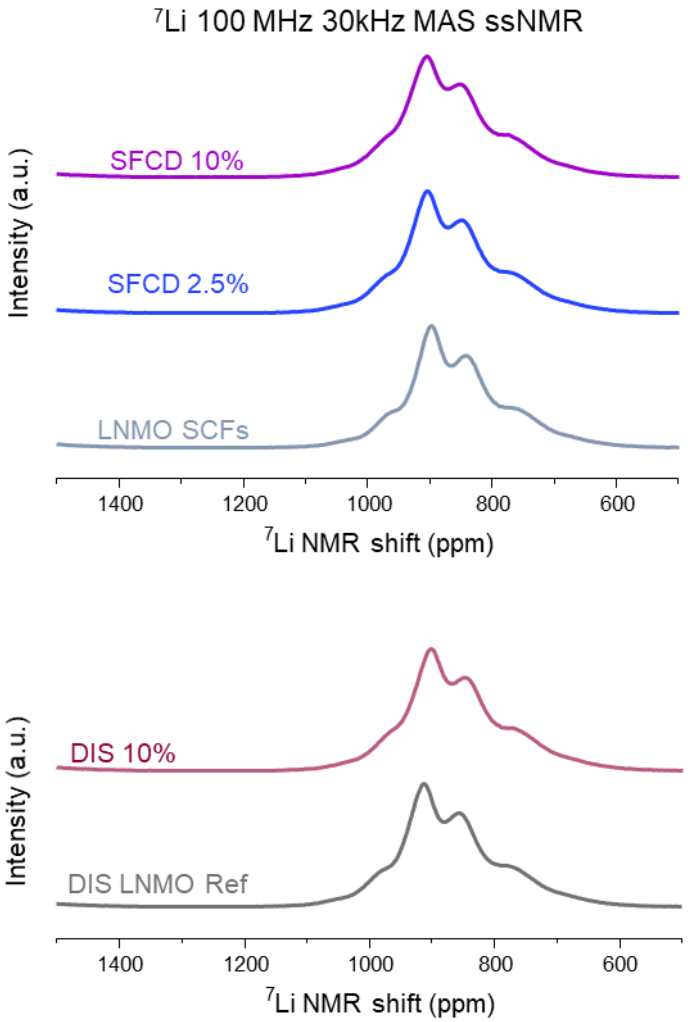

Figure S4: ^{7}Li MAS ssNMR spectra of pristine and coated materials as well as the Ref materials, those being the LNMO materials recovered from the media (solvent) in conditions in which the coatings were prepared, but without the aluminium acetylacetonate precursor. Typically, the spectrum recorded for the disordered type LNMO exhibits a broad “potatoid” shape signal centered around 900 ppm with a series of environments for Li, as those observed here.[2] When the spinel is ordered, a single narrow peak is observed as only one Li environment exists in the structure. Note also that whatever the amount of coating at the surface and the process used, the active material is not modified.

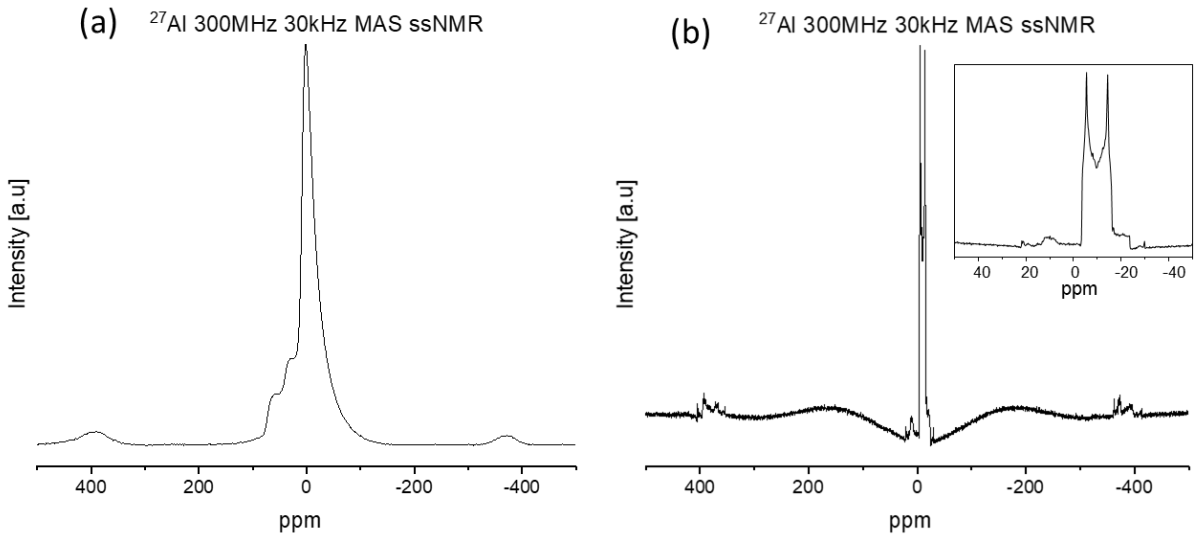

Figure S5: Comparison of ^{27}Al MAS NMR spectra of the coating material obtained as reference in SFCD conditions (a) and of the aluminium acetylacetonate precursor (b). In the later, the signal clearly exhibits a second order quadrupolar lineshape, on the contrary to the signals of ^{27}Al observed in the coatings.

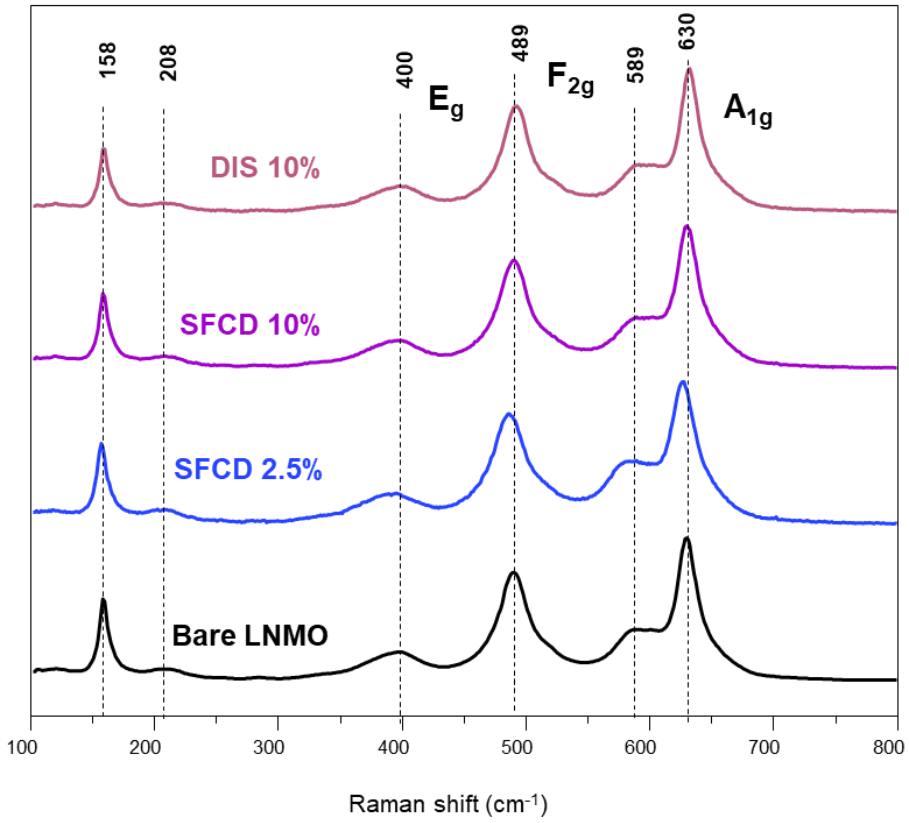

Figure S6: Raman spectra of bare and coated LNMO materials obtained with a 633 nm laser in the range of 100 to 800 cm^{-1} with an acquisition time of 10 s and 20 accumulations. Luo et al.[3] observed in their work that the presence of Al into the spinel structure induces a significant Raman peak broadening and a drop of the signal intensity. In our case, no significant difference is observed between these four spectra, there is no additional band nor real change in peak shape, which supports that the LNMO spinel phase remains unchanged after the coating processes.

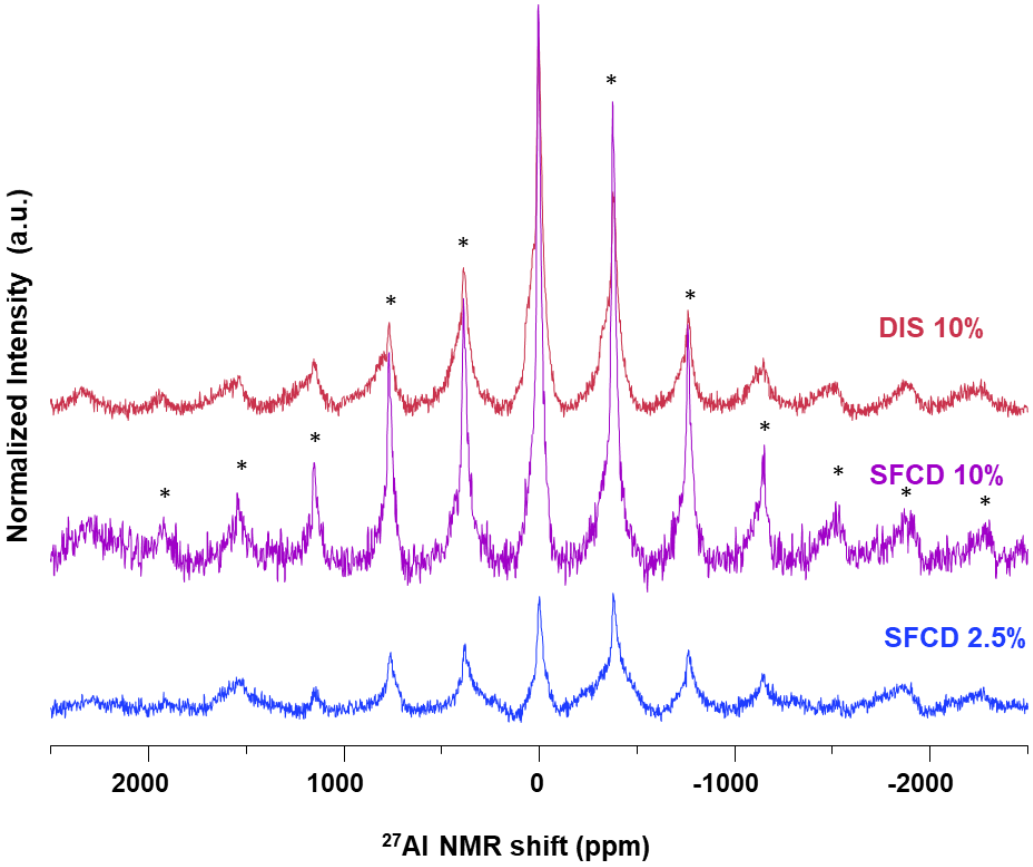

Figure S7: ^{27}Al ssNMR spectra normalised by the mass of the different samples and by the time of acquisition in order to compare semi-quantitatively the aluminium contents in the analysed samples. 13%, 10% and 5% of Al-rich material were estimated for SFCD 10%, DIS 10% and SFCD 2.5%, respectively.

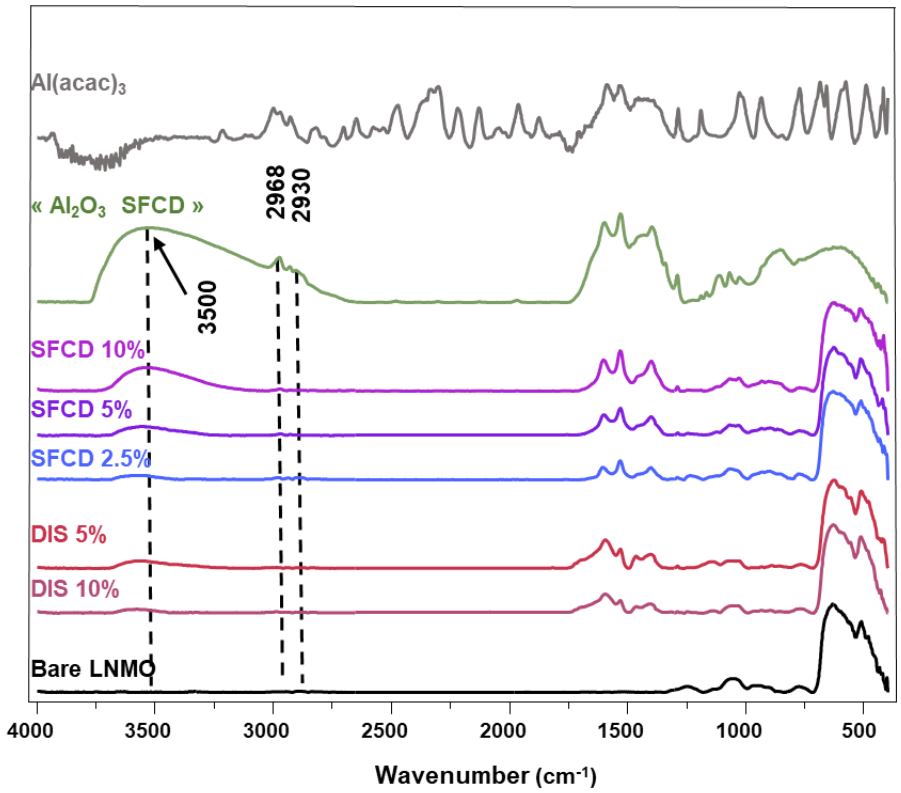

Figure S8: Extended wavenumber range FT-IR spectra, from 400 to 4000 cm^{-1}, of the bare and surface modified LNMO materials compared with references, the acetylacetonate used as precursor on one side and the Al-rich coating obtained in SFCD conditions on the other side ("Al_2O_3 SCFD").

Table S3: Assignment of bands observed in FT-IR spectra for coated materials from 400 to 4000 cm^{-1}

Wavenumber (cm^{-1})	**Assignment**
3500	ν O-H
2968, 2930	ν C-H
1597, 1527, 1469	ν C=C
1402	ν C-O
1290	δ O-H
1169, 1114, 1068	δ O-H
1030	ν Al=O
860	ν Al-O

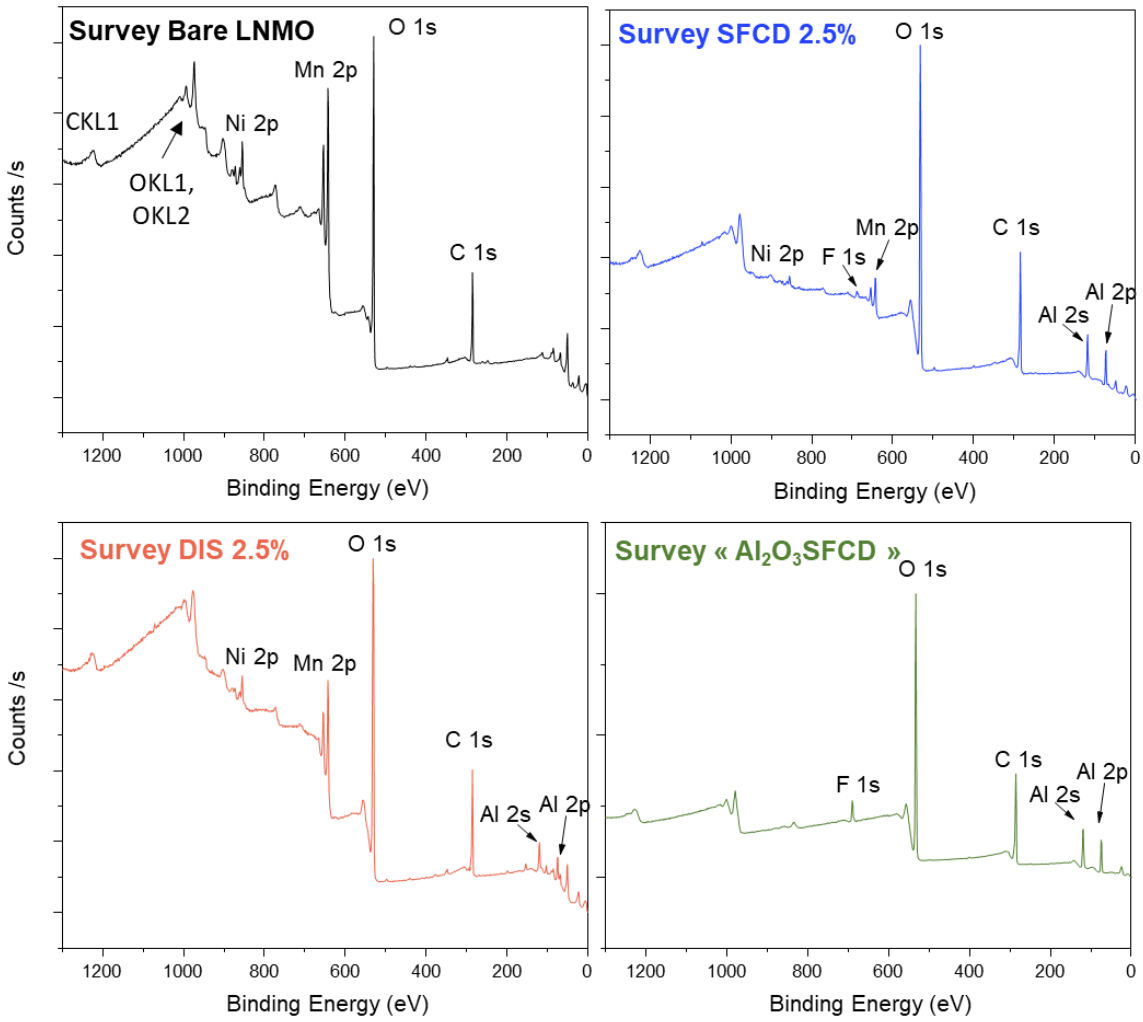

Figure S9: XPS surveys for bare and coated LNMO materials, as well as for the Al-rich coating alone obtained as reference by the SFCD process. Traces of fluorine have been detected inside SFCD materials; they were attributed to a pollution coming from the O-ring used to maintain the pressure within the synthesis reactor during the process. Indeed, this O-ring is partially composed of fluorine to reach such temperatures up to 170 °C.

Table S4: Atomic concentrations determined to be at the surface of coated materials considering the C 1s, Al 2p and O 1s spectra, with corresponding binding energies and assignments

Element	Assignment	Binding Energy (eV)	At. % SFCD 2.5%	At. % DIS 2.5%
C 1s	C-C aromatic	284.4	8.5	5.7
	CHx	285.2	14.6	15.8
	C-CO	286.2	3.5	2.3
	C-O	287.2	1.8	1.0
	C=O	288.4	1.5	1.4
	COOR	289.3	1.7	1.7
	C-F	290.3	0.6	/
Al 2p	Al-O	74.3	15.6	9.0
O 1s	Metal oxide (LNMO)	529.8	9.1	20.7
	Metal sub-oxide (LNMO)/ Al-O	530.9	7.4	7.0
	Al-O/ C=O/OH	531.9	23.2	16.6
	C-O/H_2O	533.2	7.2	4.7

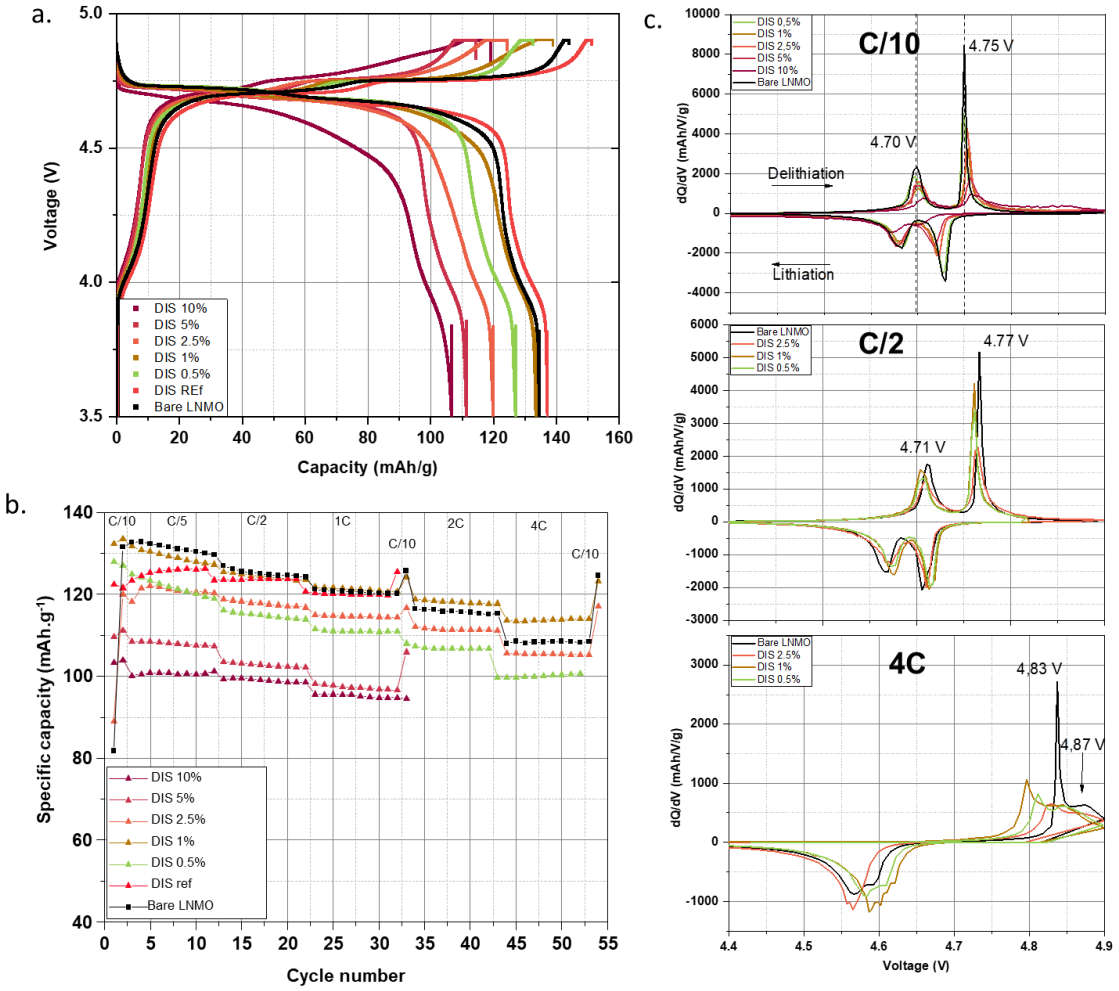

d.

Material	Reversible capacity (mA.h.g^{-1})
LNMO Pristine	135
DIS REF	119
DIS 0.5%	128
DIS 1%	133
DIS 2.5%	120
DIS 5%	111
DIS 10%	107

Figure S10: Charge-discharge curves obtained during the 1st cycle at C/10 rate (a), rate capability test from C/10 to 4C rate (b), dQ/dV curves obtained at different C-rates (C/10, C/2, 4C) (c) and comparison of reversible capacity obtained for each bare or DIS coated material (d)

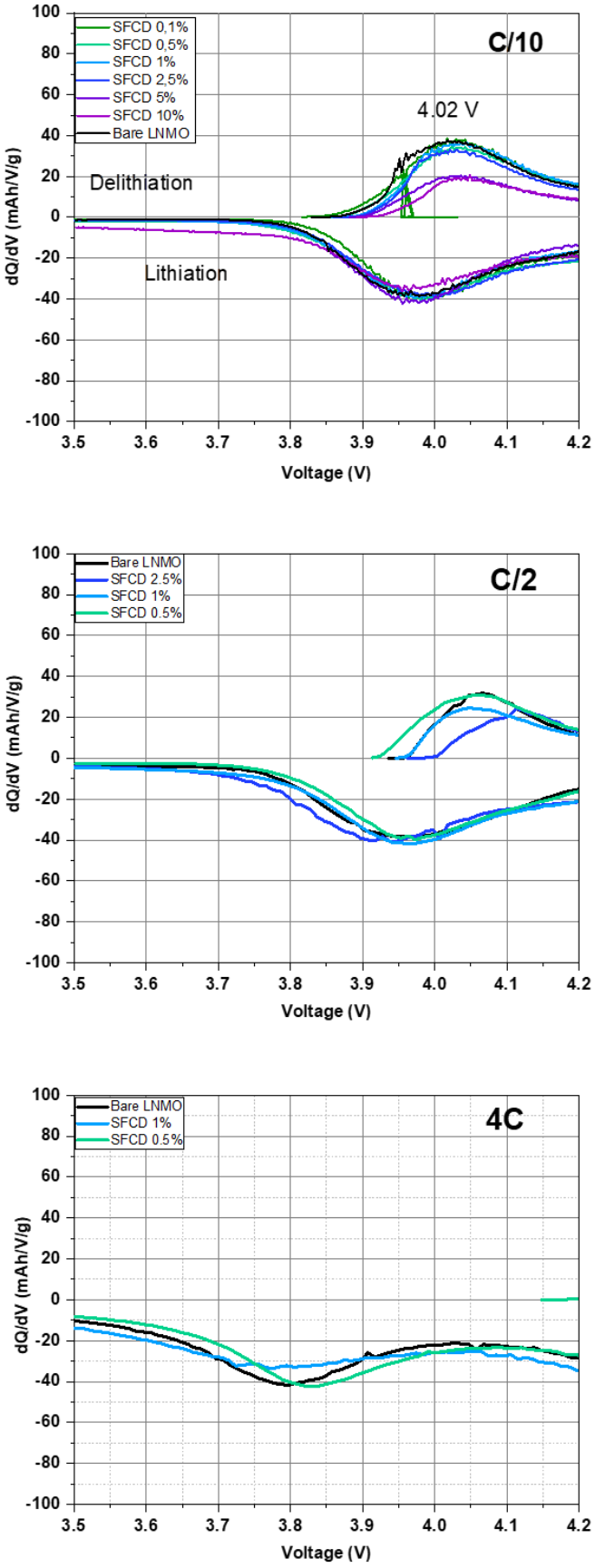

Figure S11: dQ/dV curves obtained at different rates (C/10, C/2, 4C) for bare material and coated material by SFCD focussed on the Mn^{3+}/Mn^{4+} redox activity.

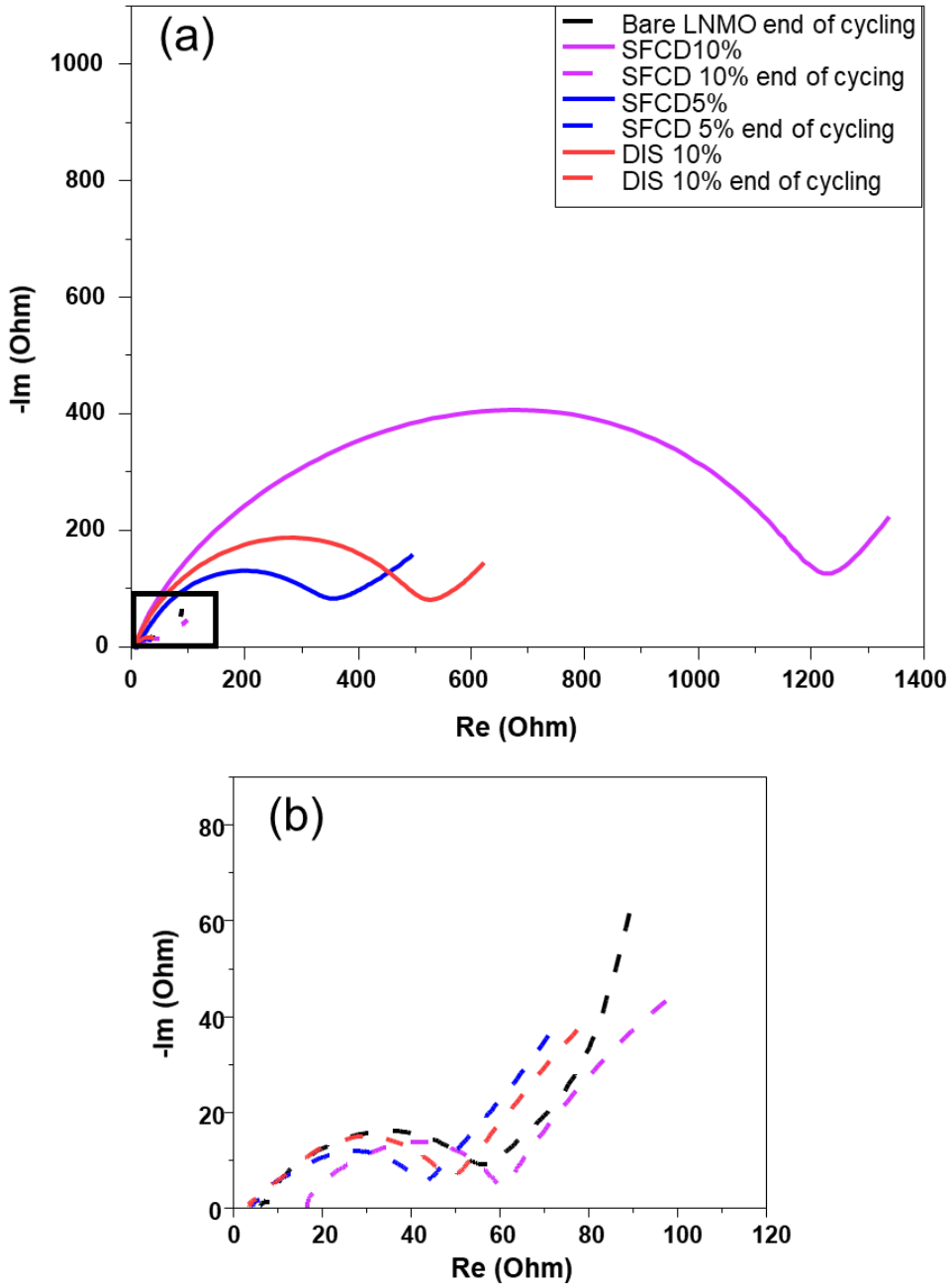

Figure S12 : Spectra obtained by Impedance Electrochemical Spectroscopy and measured directly on coin cells before cycling for the coated materials (SFCD 5%, SFCD 10% and DIS 10%), and after a rate capability test for the bare LNMO and the coated materials (a), a zoom of the lower resistance is given in (b). In Figure (a), the thicker the coating at the surface of LNMO, the bigger is the resistance before cycling. At the end of cycling the resistances obtained are similar for all the materials whatever if they are coated or not.

Table S5 : Quantification of the differences in integrated intensities observed according to the thickness of the coating layer at the surface of LNMO. These values were calculated from the derivated electrochemical curve. Indeed, for the two first columns, the relative intensity of the bare LNMO is considered as reference so equal to 1, and for the coating material, the relative intensity value was divided by the one of the bare LNMO. The final column is the ratio between the relative intensity of the Ni^{3+}/Ni^{4+} redox activity over the Ni^{2+}/Ni^{3+} redox activity in order to follow the evolution of these two peaks according the amount of coating.

	Ni^{2+}/Ni^{3+} intensity *vs.* Bare LNMO	**Ni^{3+}/Ni^{4+} intensity *vs.* Bare LNMO**	**Ni^{3+}/Ni^{4+} intensity / Ni^{2+}/Ni^{3+} intensity**
Bare LNMO	1	1	3.61
SFCD 0.1%	0.94	0.74	2.85
SFCD 0.5%	0.57	0.44	2.77
SFCD 1%	0.64	0.29	1.67
SFCD 2.5%	0.75	0.40	1.94
SFCD 5%	0.48	0.21	1.62
SFCD 10%	0.32	0.14	1.58

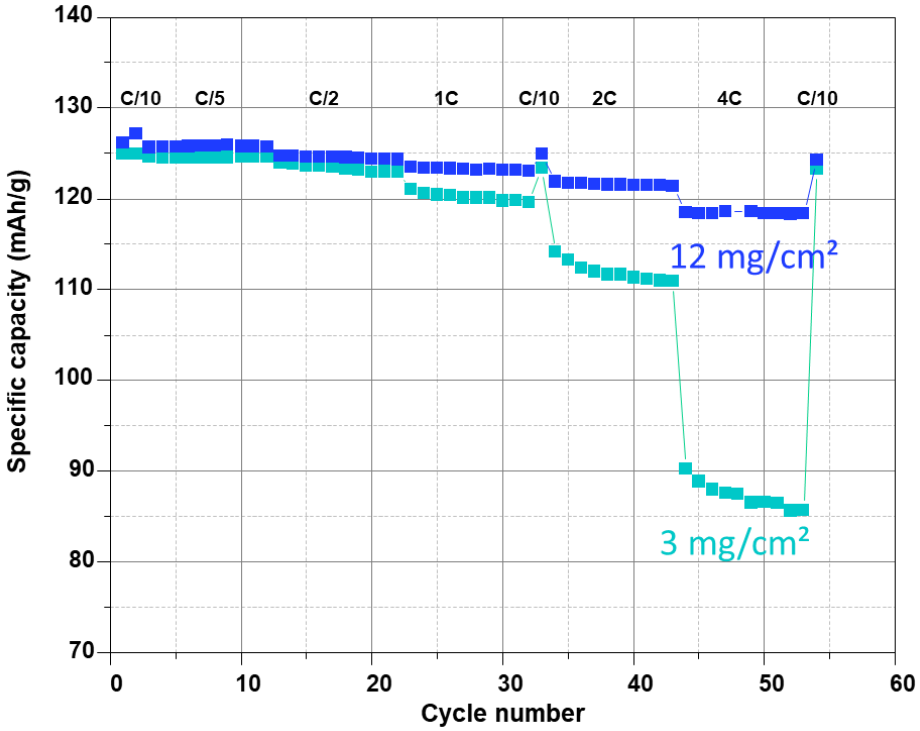

Figure S13 : Comparison of the obtained performance in rate capability test as function of the loading of the electrode for the coated material SFCD 0.5%

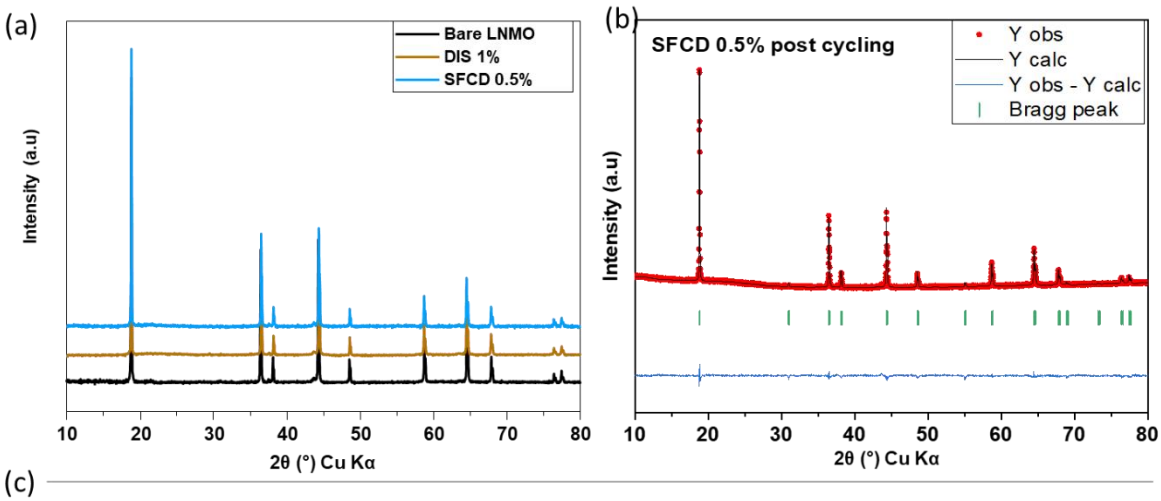

(c)

Samples	Cell parameter	Volume
Pristine LNMO	8.1714(4)	545.61(5)
SFCD 0.5% post cycling	8.1698(2)	545.30(3)
DIS 1% post cycling	8.1694(2)	545.22(2)

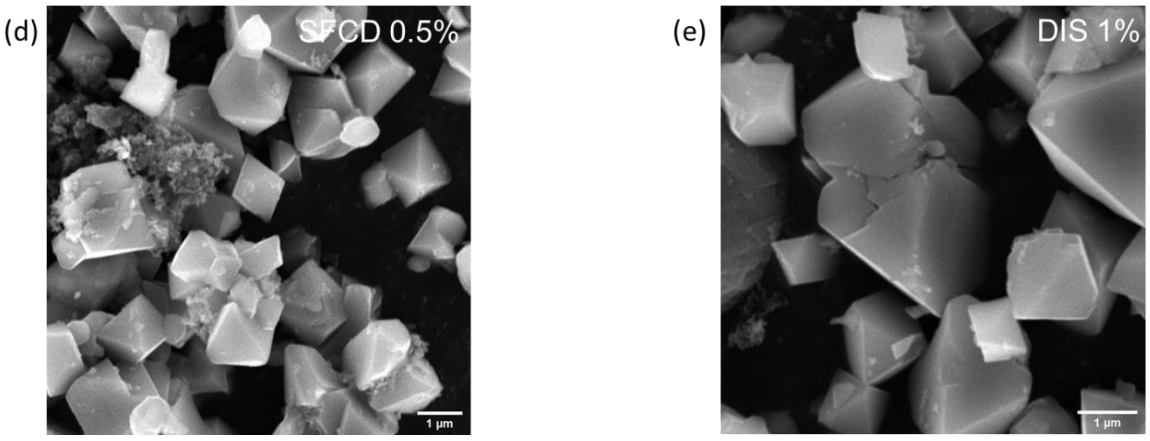

Figure S14: XRD patterns after 100 cycles at 4C for the bare and best coated LNMO materials (a), the result of SFCD 0.5% XRD pattern Le Bail refinement (b), their lattice parameters (c) and SEM images (d,e). Coin cells were disassembled in an argon atmosphere glovebox. Electrodes were washed with DMC solvent to remove lithium salt residue and scratched to recover powder. This powder is then ground finely to analyse it in capillary by XRD and by SEM.

(1) Romero Toledo, R.; Ruiz Santoyo, V.; Moncada Sánchez, C. D.; Martínes Rosales, M. Effect of Aluminum Precursor on Physicochemical Properties of Al2O3 by Hydrolysis/Precipitation Method. *Nova Sci.* **2018**, *10* (20), 83–99. https://doi.org/10.21640/ns.v10i20.1217.
(2) Duncan, H.; Hai, B.; Leskes, M.; Grey, C. P.; Chen, G. Relationships between Mn^{3+} Content, Structural Ordering, Phase Transformation, and Kinetic Properties in $LiNi_xMn_{2-x}O_4$ Cathode Materials. *Chem. Mater.* **2014**, *26* (18), 5374–5382. https://doi.org/10.1021/cm502607v.
(3) Luo, Y.; Lu, T.; Zhang, Y.; Yan, L.; Mao, S. S.; Xie, J. Surface-Segregated, High-Voltage Spinel Lithium-Ion Battery Cathode Material LiNi0.5Mn1.5O4 Cathodes by Aluminium Doping with Improved High-Rate Cyclability. *J. Alloys Compd.* **2017**, *703*, 289–297. https://doi.org/10.1016/j.jallcom.2017.01.248.